Supporting Information

Construction of graphene/cellulose aerogel embedded with UiO-66-CN for highly efficient uranium capture via electro-adsorption

*Jinhao Tian,[ab] Nan Li,[*a] Yu Luo,[ab] Hao Xing,[a] Ruidian Su [c] and Lei Wang [*a]*

a. Key Laboratory of Eco-chemical Engineering, International Science and Technology Cooperation Base of Eco-chemical Engineering and Green Manufacturing, College of Environment and Safety Engineering, Qingdao University of Science and Technology, Qingdao 266042, P. R. China

b. College of Chemistry and Molecular Engineering, Qingdao University of Science and Technology, Qingdao 266042, P. R. China.

c. College of Environmental Science and Engineering, Ocean University of China, Qingdao 266100, P. R. China

* Corresponding author.

E-mail addresses: linanhhh@qust.edu.cn (N. Li), inorchem@126.com (L. Wang).

Characterization

The microstructure of different materials was observed via a scanning electron microscope (SEM, Regulus8100, Hitachi, Japan) and a surface area analyzer (BET, ASAP2460, Micromeritics, USA). Energy dispersive spectroscopy (EDS) analysis was performed by using SEM (Regulus 8100, Hitachi, Japan) with a BRUKER XFlash 6160 detector. The crystalline characteristics of different materials were analyzed by X-ray diffraction (XRD) on a diffractometer equipment (D-MAX 2500/PC, Rigaku, Japan). Material surface chemistry was investigated by Fourier transform infrared spectroscopy (FTIR, Nicolet iS20, Thermo Fisher Scientific, USA) and X-ray photoelectron spectroscopy (XPS, ESCALAB 250Xi, Thermo Scientific, USA). The TGA curves were analyzed using a thermogravimetric analyzer (TGA, STA 449 F5 Jupiter, NETZSCH, Germany) at a heating rate of 2°C min^{-1} from 35 to 800°C under N_2 atmosphere. The concentrations of metal ions in actual water sources and simulated water were examined by inductively coupled plasma mass spectrometry (ICP-MS, 7700ICP-MS, Agilent, USA). The electrochemical performance of different electrodes was carried out by an electrochemical workstation (CHI660E Shanghai Chenhua Instrument Co., China).

Electrochemical properties.

The specific capacitance of different electrode at different scan rates was calculated from equation (1)

$$C = \frac{\int I\,dV}{2mv\Delta V} \quad (1)$$

where C (F/g) is the specific capacitance, I (A) represents current density, v (V/s) refers

to scanning rate, m (g) is adsorbent weight.

The contribution ratios of the capacitive process is calculated by equation (2)

$$i(v) = k_1 v + k_2 v^{1/2} \quad (2)$$

where k_1 and k_2 are constants.

Adsorption experimental procedure

$UO_2(NO_3)_2 \cdot 6H_2O$ was dissolved in deionized water to obtain U(VI) solutions. In electrosorption tests, a power supply unit (MS-152D, Maisheng, China) was used to provide an applied voltage. The adsorption experiments were carried out in a 50 mL solution using a three-electrode system, where a platinum plate was the counter electrode and Ag/AgCl was the reference electrode (Fig. S2). During the physicochemical adsorption, a desired amount of various materials was dosed in U(VI) solution and shaken on a shaking incubator (SHY-2A, XIUILAB, China) at the speed of 160 rpm. When the electro-/physicochemical adsorption ended, the samples were collected using 0.22 μm filters. The concentrations of U(VI) in various solutions were determined by a UV-visible spectrophotometer (UV-8000, METASH, China). The uranium electrosorption capacity and physicochemical adsorption capacity were calculated using equation (3)-(4).

$$q_e = \frac{(C_0 - C_e) \times V_s}{m} - q_{e,Nafion} \quad (3)$$

$$q_{e,Nafion} = \frac{(C_0 - C_N) \times V_s}{m_{(\text{carbon paper+Nafion})}} \quad (4)$$

Where q_e (mg/g) is the electro-/physicochemical adsorption capacity of materials and $q_{e,\ Nafion}$ (mg/g) is the electro-adsorption capacity of the Nafion electrode. In physicochemical adsorption experiments, $q_{e,\ Nafion}$ is 0. C_0 (mg/L) refers to the beginning

concentration of U(VI) solution. C_e (mg/L) and C_N (mg/L) represent the concentration of U(VI) after electro-adsorption on UiO-66-CN/GCA and pristine Nafion electrodes. V_s (L) means the solution volume. m and $m_{(\text{carbon paper+Nafion})}$ denote the mass of adsorbents and carbon paper coated Nafion, respectively.

The adsorption kinetics of uranium were evaluated by the following kinetic models.

Pseudo-first-order rate model:

$$\ln(q_e\text{-}q_t) = \ln q_e\text{-}k_1 t \quad (5)$$

Pseudo-second-order rate model:

$$\frac{t}{q_t} = \frac{t}{q_e} + \frac{1}{(k_2 q_e)^2} \quad (6)$$

Where q_t signifies the adsorption performance at time (t). k_1 and k_2 are the constants associated with the rates.

The data of adsorption isotherm experiments were fitted by the following equations.

Langmuir isotherm:

$$q_e = \frac{K_L \cdot q_{max} \cdot C_e}{1+K_L \cdot C_e} \quad (7)$$

Freundlich isotherm:

$$q_e = K_f C_e^{1/n} \quad (8)$$

Where q_{max} (mg/g) is the saturated adsorption capacity of U(VI). K_L, K_f and $1/n$ are constants.

where k_1 and k_2 are constants.

Effect of UiO-66-CN/GCA mass on U(VI) adsorption

The quantity of UiO-66-CN/GCA coated to the carbon paper is a critical aspect that significantly impacts the electrosorption effectiveness of the electrode. Fig. S3

illustrates the electrosorption ability of different electrodes at a voltage of 1 V. The electrosorption capacity exhibits an initial rise followed by a subsequent decrease as the mass of UiO-66-CN/GCA on the electrode grows. The rise in the mass of UiO-66-CN/GCA causes the coating on the electrodes to become thicker, which in turn contributes to a steady decline in the utilization of the active sites. The electrode containing 0.2 mg of UiO-66-CN/GCA achieves the highest uranium electrosorption capacity, which is selected for subsequent studies.

Reusability assay

Electro-adsorption/desorption cycle experiments of UiO-66-CN/GCA electrodes were performed to evaluate their stability and reusability. In each cycle, after electro-adsorbing in 100 mg/L uranium solution at 1.2 V for 2 h, the UiO-66-CN/GCA electrode was regenerated in different eluents (1 M NaCl, 0.5 M Na_2CO_3, 1 M Na_2CO_3) with a reverse voltage of 1.2 V for 2 h. The desorbed electrodes were gently rinsed with water and then air-dried for the subsequent cycle.

Selectivity tests

Uranium selectivity of UiO-66-CN/GCA was tested via both physicochemical adsorption and electrosorption in simulated solutions containing UO_2^{2+}, VO_3^-, Ba^{2+}, Ca^{2+}, Cu^{2+}, Mg^{2+}, Na^+. The concentration of each ion before and after adsorption was determined by ICP-MS. The selectivity of UiO-66-CN/GCA for uranium was evaluated as follows:

$$K_{d(M)} = q_e / C_e \tag{9}$$

$$\alpha_M = K_{d(U)} / K_{d(M)} \tag{10}$$

where $K_{d(M)}$ refers to the distribution coefficient, α_M is the selectivity coefficient, and M represents metal ions.

DFT calculation

To investigate the enhancing impact of the electric field on uranium adsorption by UiO-66-CN/GCA, molecular dynamics simulations were performed with the GROMACS software, employing the GAFF.[1] The water molecules were described with the TIP3P mode and the initial model was constructed (Fig. S4). An electric field of 0.5 V/nm was applied along the z-axis and a 1000 ps NVT simulation was subsequently conducted. The simulations maintained a constant temperature of 298 K using the V-rescale thermostat approach,[2] with a cutoff distance of 1.2 nm.[3] The LINCS algorithm was employed to constrain bonds involving hydrogen atoms with a time step of 2 fs.[4] Long-range electrostatics were computed via the Particle Mesh Ewald (PME) method and visualization of the trajectory was generated using the VMD software.[5]

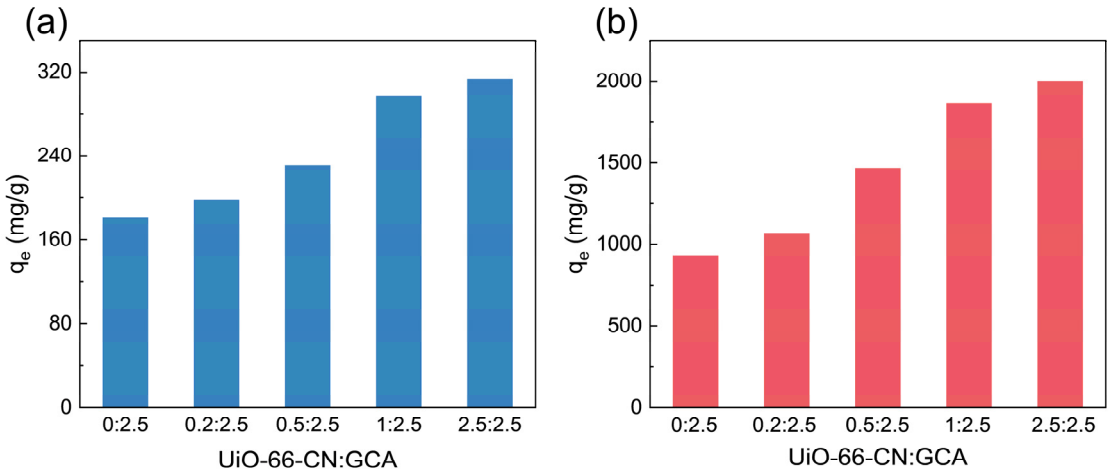

Figure S1. (a) Physicochemical adsorption and (b) electrosorption of UiO-66-CN/GCAs with different ratios.

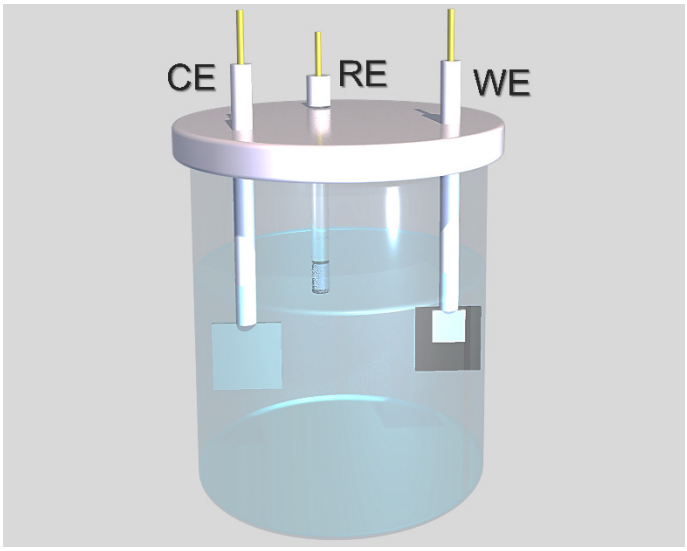

Figure S2. Three-electrode system (WE: UiO-66-CN/GCA, RE: Ag/AgCl, CE: Pt).

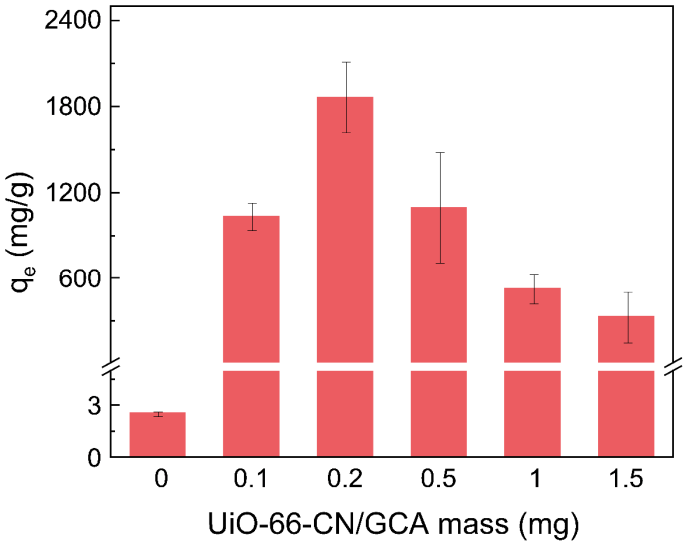

Figure S3. Electro-adsorption performance of electrodes with different masses of UiO-66-CN/GCA.

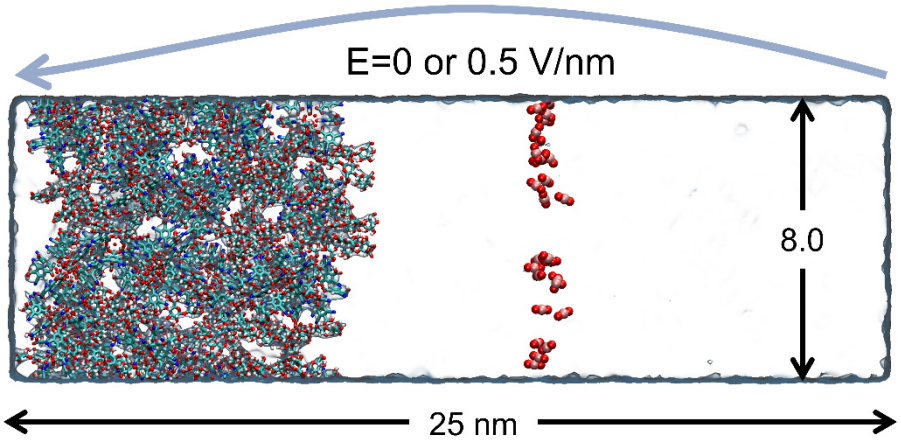

Figure S4. Construction of initial molecular dynamics model.

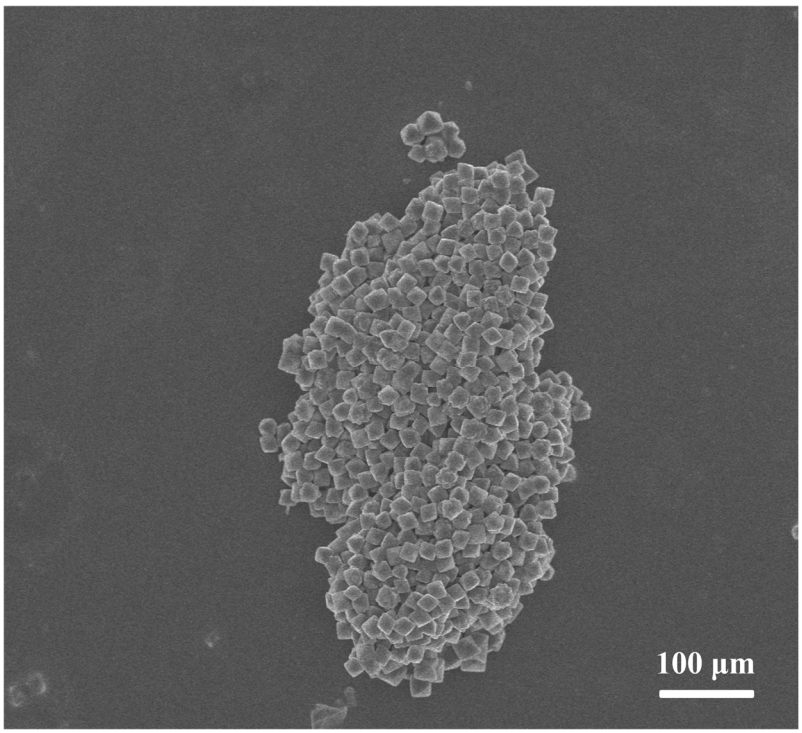

Figure S5. SEM image of UiO-66-CN.

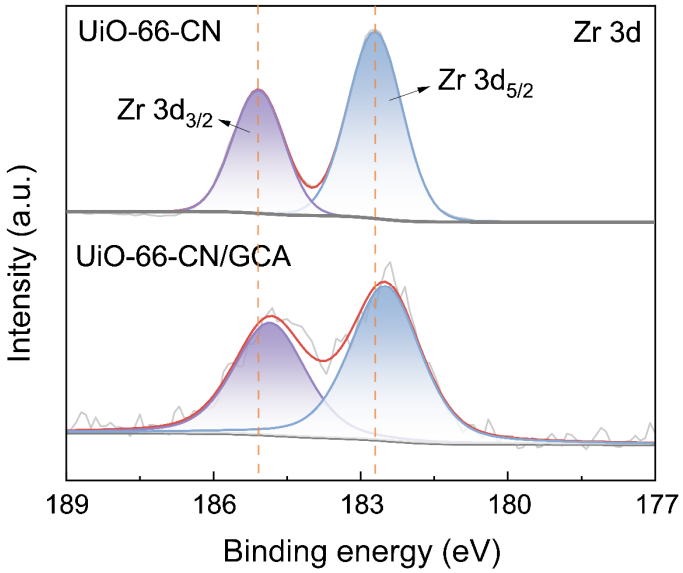

Figure S6. XPS spectra of Zr 3d for UiO-66-CN and UiO-66-CN/GCA.

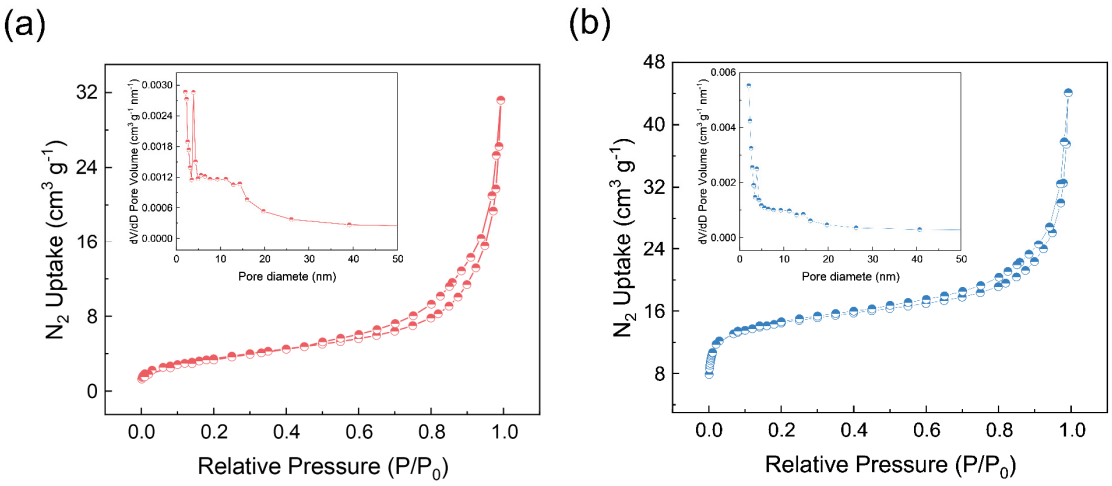

Figure S7. The N_2 adsorption/desorption isotherms and pore size distribution of (a) GCA and (b) UiO-66-CN/GCA.

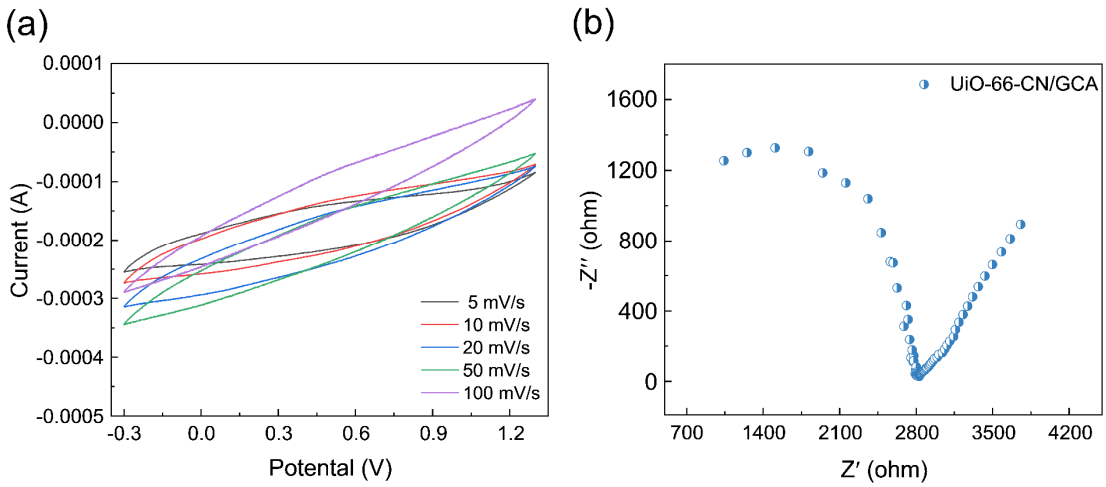

Figure S8. (a) CV curves and (b) Nyquist plots of UiO-66-CN/GCA in a three-electrode system using 100 mg/L U(VI) solution as electrolyte.

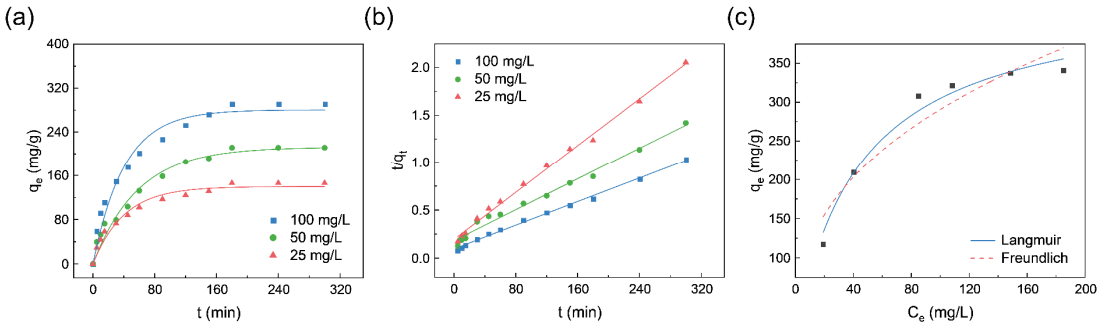

Figure S9. (a) Pseudo-first-order and (b) pseudo-second-order kinetics for uranium physicochemical adsorption of UiO-66-CN/GCA. (c) Physicochemical adsorption isotherms of UiO-66-CN/GCA.

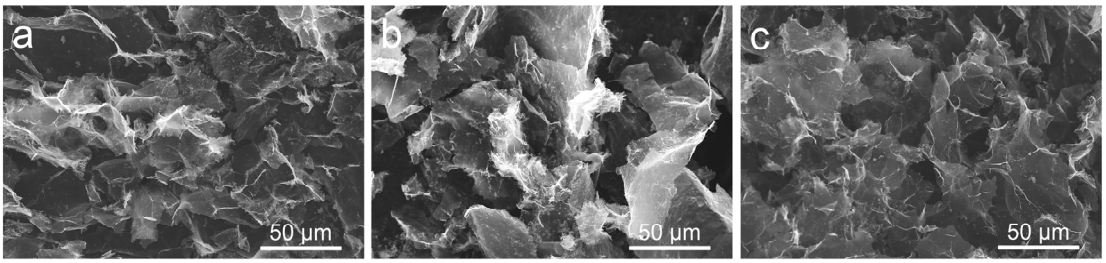

Figure S10. SEM images of UiO-66-CN/GCA (a) after the first desorption, (b) after the second desorption and (c) after the third desorption in three electrosorption/desorption cycles.

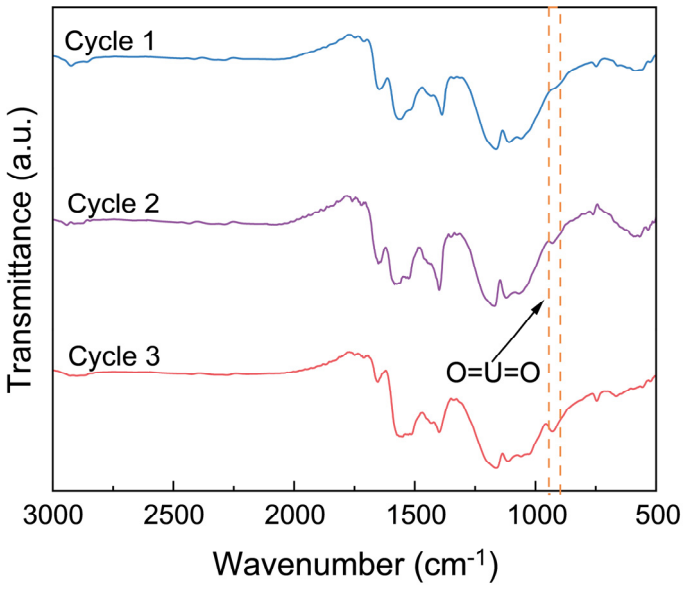

Figure S11. FTIR spectra of UiO-66-CN/GCA after each cycle of desorption in three electrosorption/desorption cycles.

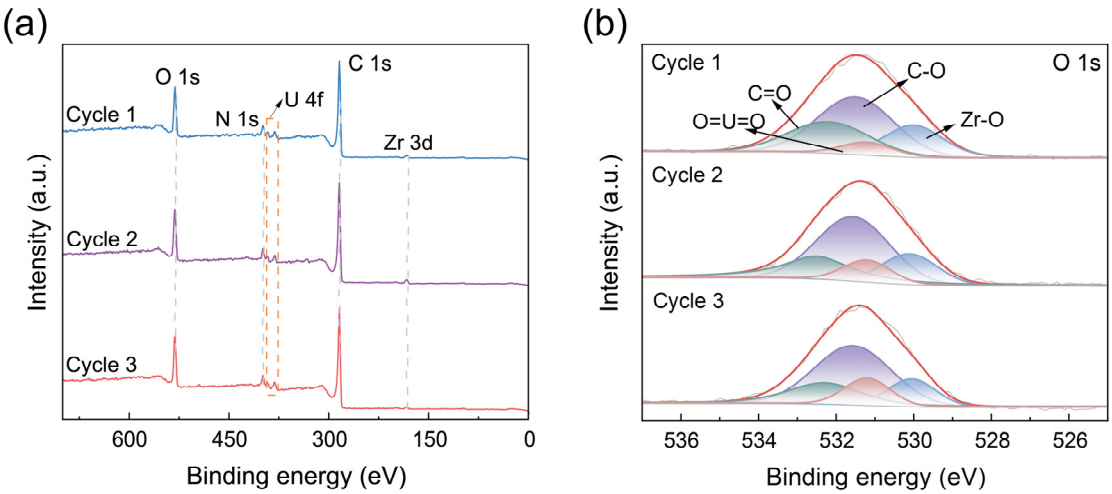

Figure S12. (a) XPS survey spectra and (b) XPS spectra of O 1s for UiO-66-CN/GCA after desorption in three electrosorption/desorption cycles.

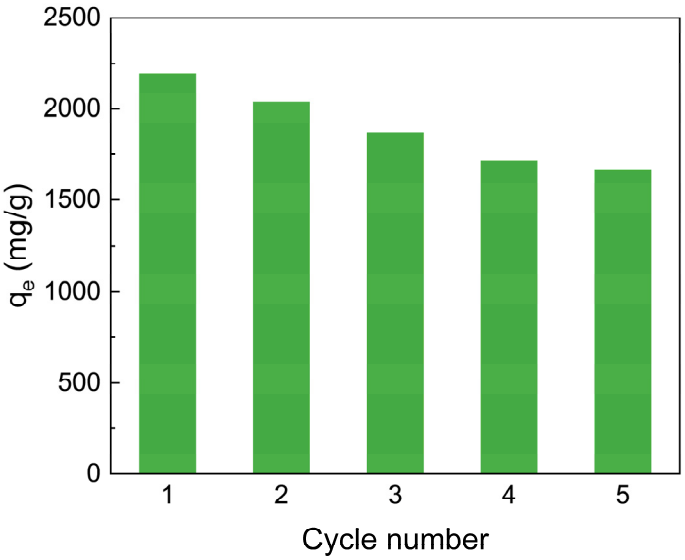

Figure S13. Reusability of UiO-66-CN/GCA in highly enriched uranium.

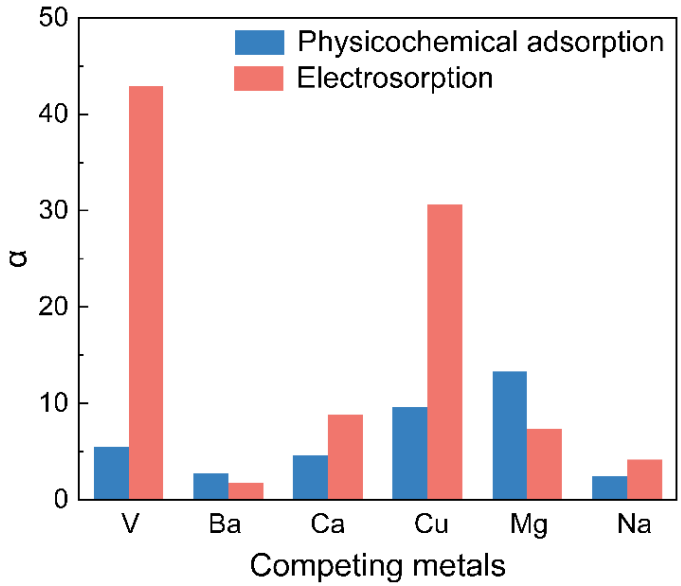

Figure S14. Selectivity coefficients for different metal ions in simulated water.

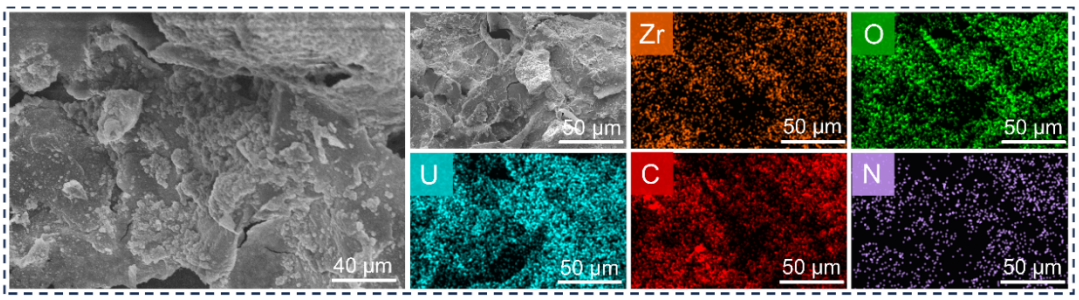

Figure S15. SEM images and EDS mapping of UiO-66-CN/GCA-U.

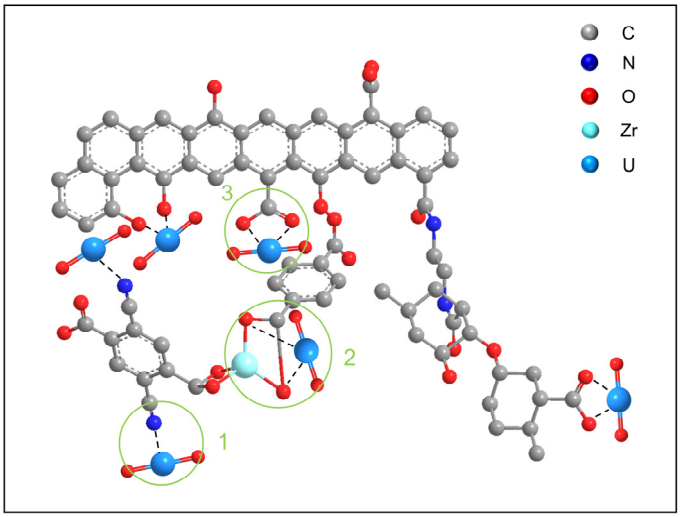

Figure S16. Adsorption mechanisms of UiO-66-CN/GCA.

Table S1. Material electrosorption uranium cost analysis.

UiO-66-CN:GCA	q_e (mg/g)	Cost ($/mg-U)
0:2.5	934.6	0.0299
0.2:2.5	1068.1	0.0589
0.5:2.5	1468.6	0.0783
1:2.5	1869.1	0.1043
2.5:2.5	2002.6	0.2297

Table S2. The proportions of different elements of UiO-66-CN/GCA by EDS.

Elements	Mass (%)	Atom (%)
C	61.43	68.90
N	9.54	9.18
O	25.40	21.38
Zr	3.63	0.54

Table S3. Curve fitting results of C 1s XPS spectra.

Samples	Peak	Binding energy (eV)	Area	Relative content (%)
GCA	C-C/C=C	284.80	17105.60	64.99
	C-O	286.31	5772.16	21.93
	O=C-O	288.40	2417.97	9.18
	C-N	285.80	1020.87	3.90
UiO-66-	C-C/C=C	284.80	16228.25	56.08
CN/GCA	C-O	286.00	7214.18	24.94
	O=C-O	288.60	2684.93	9.28
	C-N	285.80	1110.50	3.84
	C≡N	287.20	1487.44	5.86

Table S4. Relative ratios of elements determined from XPS.

Materials	Atomic ratio (%)			
	C	N	O	Zr
GA	83.47	4.63	14.93	
UiO-66-CN	55.82	2.01	36.69	5.48
UiO-66-CN/GCA	78.60	6.17	14.93	0.30

Table S5. Porous structure parameters of GCA and UiO-66-CN/GCA.

Adsorbent	S_{BET} (m^2/g)	V_{tot} (cm^3/g)	D_{ave} (nm)
GCA	12.7341	0.024272	12.8354
UiO-66-CN/GCA	45.7204	0.040718	11.9184

S_{BET}: specific surface area V_{tot}: total pore volume D_{ave}: average pore diameter

Table S6. Parameters for kinetic models of U(VI) physicochemical adsorption by UiO-66-CN/GCA.

Conditions	Pseudo-first-order		Pseudo-second-order	
	Physicochemical adsorption			
25 mg/L	k_1 (min^{-1})	2.491×10^{-2}	k_2 ($g\cdot mg^{-1}\cdot min^{-1}$)	1.966×10^{-4}
	q_e (mg/g)	139.7	q_e (mg/g)	162.3
	R^2	0.9636	R^2	0.9955
50 mg/L	k_1 (min^{-1})	1.713×10^{-2}	k_2 ($g\cdot mg^{-1}\cdot min^{-1}$)	9.065×10^{-5}
	q_e (mg/g)	212.3	q_e (mg/g)	247.5
	R^2	0.9693	R^2	0.9839
100 mg/L	k_1 (min^{-1})	2.457×10^{-2}	k_2 ($g\cdot mg^{-1}\cdot min^{-1}$)	9.930×10^{-5}
	q_e (mg/g)	280.4	q_e (mg/g)	324.7
	R^2	0.9628	R^2	0.9955
	Electrosorption			
25 mg/L	k_1 (min^{-1})	3.617×10^{-2}	k_2 ($g\cdot mg^{-1}\cdot min^{-1}$)	8.321×10^{-5}
	q_e (mg/g)	909.7	q_e (mg/g)	724.6
	R^2	0.9697	R^2	0.9873
50 mg/L	k_1 (min^{-1})	4.419×10^{-2}	k_2 ($g\cdot mg^{-1}\cdot min^{-1}$)	7.681×10^{-5}
	q_e (mg/g)	909.8	q_e (mg/g)	1000.0
	R^2	0.9797	R^2	0.9923
100 mg/L	k_1 (min^{-1})	6.402×10^{-2}	k_2 ($g\cdot mg^{-1}\cdot min^{-1}$)	5.118×10^{-5}
	q_e (mg/g)	1996.0	q_e (mg/g)	2129.0
	R^2	0.9857	R^2	0.9949

Table S7. Isotherm parameters for U(VI) electrosorption onto UiO-66-CN/GCA.

Isotherm models	Parameters	
Langmuir	q_{max} (mg/g)	3092.3
	K_L (L/mg)	1.47×10^{-2}
	R^2	0.9459
Freundlich	$1/n$	0.4227
	K_f ((mg/g) L/mg$^{1/n}$)	247.83
	R^2	0.8657

Table S8. Isotherm parameters for U(VI) physicochemical onto UiO-66-CN/GCA.

Isotherm models	Parameters	
Langmuir	q_{max} (mg/g)	442.7
	K_L (L/mg)	2.21×10^{-2}
	R^2	0.9722
Freundlich	$1/n$	0.3922
	K_f ((mg/g) L/mg$^{1/n}$)	47.74
	R^2	0.8822

Table S9. Comparison with other electric-adsorbents reported in previously reported works.

Adsorbents	Equilibrium time (h)	q_{max} (mg/g)	Applied voltage (V)	Optimal pH	Actual environmental adsorption performance (mg/g)	adsorption capacity after five cycles (mg/g)	Reference
CMPC	5	410.3	1.2	-	-	351.6	[6]
PEI/GOA	6	419.7	1.2	9	-	346.6	[7]
CMM	5	582.5	1.2	-	-	-	[8]
BBC/PPy-3	1.5	402.5	0.9	4.5	-	-	[9]
MoS_2/GO-H	4	805.6	1.2	5	-	700.8	[10]
CMP-0.10	1.6	339.5	0.9	4	-	-	[11]
GO/PPy-0.2	2.5	246.5	0.9	4	-	-	[12]
AGMM	3	831.5	1.5	5	-	65.0	[13]
CC-AO	12.5	989.5	2.5	2	-	-	[14]
PA-PPy/CF	10	1562.0	5.0	5	-	709.6	[15]
F-TC	23	626.0	0.7	5	-	-	[16]
BSA@CFF	12.5	2850.0	2.6	6	Seawater: 6.5	750.0	[17]
MCA	1.5	1826.4	1.0	5	Seawater: 13.82	1066.0	[18]
UiO-66-CN/GCA	1.5	3092.3	1.2	6	Seawater: 110.1 Lakes and rivers: 23.0	1132.4	This work

Table S10. Relative elemental ratios of UiO-66-CN/GCA after each cycle as determined by XPS.

Samples	Atomic ratio (%)				
	C	N	O	Zr	U
Cycle 1	77.64	5.78	16.18	0.26	0.14
Cycle 2	77.99	4.99	16.48	0.38	0.16
Cycle 3	76.49	6.68	16.44	0.21	0.18

Table S11. Curve fitting results of O 1s XPS spectra of UiO-66-CN/GCA after desorption in three electrosorption/desorption cycles.

Samples	Peak	Binding energy (eV)	Area	Relative content (%)
Cycle 1	C-O	531.5	9545.17	45.58
	C=O	532.2	5506.55	26.29
	Zr-O	530.0	4531.87	21.64
	O=U=O	531.2	1359.08	6.49
Cycle 2	C-O	531.56	13226.28	48.68
	C=O	532.5	6275.98	23.10
	Zr-O	530.1	4780.93	17.59
	O=U=O	531.2	2885.07	10.63
Cycle 3	C-O	531.57	14040.58	51.22
	C=O	532.3	5541.93	20.22
	Zr-O	530.05	4015.18	14.65
	O=U=O	531.2	3813.46	13.91

Table S12. Concentrations of each metal ion before and after adsorption of UiO-66-CN/GCA in simulated water.

Metal	C_0 (μg/L)	Physicochemical adsorption		Electrosorption	
		C_e (μg/L)	q_e (mg/g)	C_e (μg/L)	q_e (mg/g)
U	301.6	219.7	40.9	250.1	257.5
V	206.8	193.5	6.6	205.9	4.5
Ba	288.3	253.6	17.3	260.9	137.0
Ca	336.3	311.1	12.6	329.3	35.0
Cu	231.0	222.4	4.3	229.6	7.0
Mg	268.7	261.4	3.6	262.0	33.5
Na	280.3	243.0	18.6	268.6	58.5

Table S13. The distribution coefficient (K_d) and selectivity coefficient (α) of UiO-66-CN/GCA for different metals in simulated seawater.

Metal	Physicochemical adsorption		Electrosorption	
	K_d	α	K_d	α
U	186.40	1.00	1029.60	1.00
V	34.10	5.46	21.85	47.20
Ba	68.41	2.72	525.10	1.96
Ca	40.50	4.60	106.20	9.69
Cu	19.33	9.65	30.48	33.70
Mg	13.96	13.30	127.80	8.05
Na	76.74	2.43	223.90	4.59

Table S14. Uranium concentration before and after adsorption in different river and lake waters.

Water samples	C_0 (μg/L)	C_e (μg/L)	q_e (mg/g)
Xiangmi Lake Park	1.965	1.757	10.4
Shigou Park	1.915	1.572	17.2
Licun River	2.238	2.594	17.8
Zhangcun River	2.867	2.407	23.0

References

1. J. Wang, R. M. Wolf, J. W. Caldwell, P. A. Kollman and D. A. Case, *J. Comput. Chem.*, 2004, **25**, 1157-1174.
2. G. Bussi, D. Donadio and M. Parrinello, *J. Chem. Phys.*, 2007, **126**, 014101.
3. M. Parrinello and A. Rahman, *J. Appl. Phys.*, 1981, **52**, 7182-7190.
4. B. Hess, H. Bekker, H. J. C. Berendsen and J. G. E. M. Fraaije, *J. Comput. Chem.*, 1997, **18**, 1463-1472.
5. W. Humphrey, A. Dalke and K. Schulten, *J. Mol. Graph.*, 1996, **14**, 33-38.
6. Q. Hu, D. Wang, J. Liang, Z. Liu and J. Li, *Sep. Purif. Technol.*, 2024, **330**, 125494.
7. Q. Ren, Y. Wang, Y. Wang, Z. Feng, H. Jiang, Y. Liu, D. Yuan, C. Wang and Y. Li, *Sep. Purif. Technol.*, 2025, **352**, 128191.
8. Y. Zhang, J. Zhou, D. Wang, R. Cao and J. Li, *Chem. Eng. J.*, 2022, **430**, 132702.
9. H. Shehzad, M. T. Shuang, J. Chen, Z. Liu, A. Sharif, Z. H. Farooqi, E. Ahmed, R. Begum, L. Zhou, J. Ouyang, A. Irfan, A. R. Chaudhry, S. Shaukat and U. Hussain, *J. Environ. Chem. Eng.*, 2024, **12**, 111957.
10. Y. Liu, J. Zhao, T. Bo, R. Tian, Y. Wang, S. Deng, H. Jiang, Y. Liu, G. Lisak, M. Chang, X. Li and S. Zhang, *Small*, 2024, 2401374.
11. Y. Liu, L. Zhou, J. Ouyang, X. Ao, M. Shuang and A. A. Adesina, *Sep. Purif. Technol.*, 2024, **334**, 125989.
12. M. Shuang, L. Zhou, Y. Liu, H. Yu, X. Ao, J. Ouyang, Z. Liu, H. Shehzad and A. A. Adesina, *J. Environ. Chem. Eng.*, 2023, **11**, 111498.
13. W. Tang, D. Li, X. Zhang, F. Guo, C. Cui, M. Pan, D. Zhang, J. Li and X. Xu, *Sep. Purif. Technol.*, 2023, **319**, 124087.
14. M. Pan, C. Cui, W. W. Tang, Z. R. Guo, D. X. Zhang, X. Y. Xu and J. Y. Li, *Sep. Purif. Technol.*, 2022, **281**, 119843.
15. J. Huang, Z. Liu, D. Huang, T. Jin and Y. Qian, *J. Hazard. Mater.*, 2022, **433**, 128775.
16. P. Zhang, L. Wang, Z. Huang, J. Yu, Z. Li, H. Deng, T. Yin, L. Yuan, J. K. Gibson, L. Mei, L. Zheng, H. Wang, Z. Chai and W. Shi, *ACS Appl. Mater. Interfaces*, 2020, **12**, 15579-15587.
17. H. Ye, T. Li, Y. Huang, J. Jin, J. Fei, M. Wu and J. Yao, *Chem. Eng. J.*, 2023, **451**, 138615.
18. N. Shi, J. Wu, X. Zhi, N. Li and Z. Wang, *Chem. Eng. J.*, 2023, **476**, 146563.